Numerical modelling of ice

Mechanical behaviour of ice under high strain rates

Ma, Dayou; Li, Xi; Manes, Andrea; Li, Yulong

DOI
10.1016/j.ijimpeng.2022.104375

Publication date
2023

Document Version
Final published version

Published in
International Journal of Impact Engineering

International Journal of Impact Engineering 172 (2023) 104375

Contents lists available at ScienceDirect

International Journal of Impact Engineering

journal homepage: www.elsevier.com/locate/ijimpeng

Numerical modelling of ice: Mechanical behaviour of ice under high strain rates

Dayou Ma [a,b,*], Xi Li [a,c], Andrea Manes [b], Yulong Li [a,*]

[a] School of Civil Aviation, Northwestern Polytechnical University, Suzhou, China
[b] Politecnico di Milano, Department of Mechanical Engineering, via la Masa, 1, Milan 20156, Italy
[c] Structural Integrity & Composites Group, Faculty of Aerospace Engineering, Delft University of Technology, Kluyverweg 1, 2629HS, Netherlands

ARTICLE INFO

Keywords:
Johnson-Cook model
Johnson-Holmquist II model
Ice projectile
Damage phenomena
Ballistic impact

ABSTRACT

Ice impact is quite common and may become critical especially if it involves the transportation sector. Simulation tools may help in the structural design phase to increase the ability to withstand this kind of impact and/or to analyse the effect under extreme weather conditions. Such tools require an accurate description of the mechanical behaviour and therefore a detailed investigation about the dynamic mechanical properties of ice is of great interest. In the present work, material characterizations of ice, including tensile and compressive tests, were carried out under different strain rates. Two different material models (i.e., the modified Johnson-Cook model and Johnson-Holmquist II model) were calibrated. Then, impact tests using ice as a projectile with aluminium panels as a target were conducted to validate the material models of ice under impact loading. Furthermore, the replication effect of ice projectiles was investigated under different impact energies based on the mechanical responses and damage phenomena of ice for both models. Results showed that while both models are able to provide reliable predictions of the impact behaviour of ice projectiles, the Johnson-Holmquist II model presents a better performance as impact energy increases.

1. Introduction

Ice impact is always regarded as a destructive hazard in many fields, such as civil, marine, and aerospace engineering. Understanding and modelling the dynamic mechanical behaviour of ice, especially under impact loading, is of great interest, which can help the design and optimization of structures to resist ice impact. Despite the environmental sensitivity of ice [1–3], experimental investigations considering various strain rates have been widely conducted to understand the mechanical behaviour of ice and establish a reliable material model. However, besides environmental factors, one important extra concern that should be stressed is that the mechanical properties of ice are significantly affected by the type of water: fresh, atmospheric, river, sea and distilled [1,4–7]. Among these, ice generated from distilled water presents the highest strength [5]. Therefore, most experimental analysis, especially impact cases, utilised ice projectiles made from distilled water, for the purpose of structural design with high safety factors.

For tensile tests, to avoid ice melting at the contact region with the clamps, ice samples should be assembled with especially designed clamps before testing at low temperature [4]. Spalling tests with split Hopkinson pressure bar (SHPB) can provide precise experimental data about tensile strength of ice with the assistance of an high-speed camera [8,9]. However, the correct interpretation of the failure modes, due to different stress states, is complex with transparent material like ice. On the other hand, Brazilian tests, which were originally designed for brittle materials, are also capable to measure tensile strength of ice [2,6], as long as it is validated by the initial central failure of samples [10]. In particular, Brazilian tests by means of SHPB have been regarded as an effective way to obtain the tensile strength under high strain rates [3,5]. According to the existing experimental results [3,4,6], tensile strength of ice is around 1.0 MPa under the quasi-static conditions, while limited increase on the strength can be found with an increase of the strain rate and lowering of the temperature.

Unlike tensile tests, compressive experiments are much easier to carry out. At intermediate strain rates (~10 /s), compressive strength of ice increases compared with that in the static condition [11]. Regarding higher loading rates, SHPB is usually employed [13–16], as it can achieve a strain rate range from 10 /s up to 2600 /s under compressive loading conditions. Such a strain rate range is similar to those of impact cases (10^1 – 10^3 /s). However, even though loading with a constant

* Corresponding authors at: School of Civil Aviation, Northwestern Polytechnical University, Suzhou, China.
E-mail addresses: Dayou.ma@polimi.it (D. Ma), liyulong@nwpu.edu.cn (Y. Li).

https://doi.org/10.1016/j.ijimpeng.2022.104375
Received 29 March 2022; Received in revised form 15 July 2022; Accepted 5 September 2022
Available online 6 September 2022

strain rate is hard to achieve when the strain rate is close to 1000 /s [12,13], the shaping of an incident wave has been studied [13,14].

Regarding ice impact tests, the impact loading profile and the collapse of ice projectiles are usually measured and captured [15,16]. Additionally to the shape, (e.g. sphere [17,18] and cylinder [15]), also the impact velocity [19], and the size [20] of ice projectiles are considered main factors for the study of ice impact. However, test data always shows a large scatter, due to the variation of ice projectiles induced during their manufacturing process and the uncertainty of the measurement [17]. Besides controlling the manufacture process, efforts have also been made to improve the accuracy of measurements. For example, Pernas-Sánchez et al. [20] utilized a mass-spring analogous system on a load cell to measure the impact force provided by the ice projectile, while high-speed cameras were used to record the impact process [15,16,19]. Both rigid [15,21] or aluminium targets [18], which have predictable material models, are used to inversely reproduce the ballistic behaviour of ice projectiles. In comparison to monitoring ice projectiles themselves, the recording of the mechanical response of the targets is more practical and applicable thanks to advanced measurement methods [21,22], such as digital image correlation (DIC) techniques.

Based on material tests under various strain rates, the material model of ice can be calibrated, which is helpful for the simulation of ice impact. Considering the strain-rate sensitivity of ice, a theoretical model with strain-rate parameters can be used [23], while typical semi-empirical material models, like Johnson-Cook constitutional model [24] and Zhu–Wang–Tang model [25], are capable to simulate the mechanical behaviour of ice under high loading rates. While the ice projectile with high impact velocities can be accurately captured by the equation of state (EOS), material models including EOS also present good capabilities of ice impact simulation [26–28]. However, determining the parameters of EOS is difficult because planetary impact tests need to be performed, which require hyper impact velocity of ice projectiles and an extremely accurate monitoring system [29,30]. Besides, advanced numerical methodologies, such as the particle-subdomain method [31] and smoothed particle hydrodynamics [32], which always use rate-dependent material properties as input, are more appropriate for replicating the mechanical behaviour of ice impact, especially the failure process. Meanwhile, micromechanics also provide a new insight for the modelling of ice, as they can provide reliable mechanical behaviour considering the effect of temperature and strain rate with a microscale kinematic and constitutional relationship [33]. However, the capabilities of these numerous material s models and numerical methodologies with regards to modelling ice projectiles under various impact velocities are still not clear and are hence the main focuses of the present work.

In the current work, experimental activities, including tensile and compressive loading conditions, considering different strain rates, were conducted to characterize the mechanical properties of ice. Based on experimental data, two different material models, the modified Johnson-Cook and the Johnson-Holmquist II models, were calibrated to replicate the mechanical properties of ice as a projectile. In order to assess these two material models, impact tests with ice projectiles versus aluminium targets were carried out. Through comparisons between experimental data and simulated results of ice impact cases, both material models were validated with respect to failure phenomena and residual velocities.

2. Experiments

2.1. Sample preparation

Two differently shaped ice samples were prepared for the current study: an ice cylinder used for material characterizations, including tensile and compressive tests and an ice sphere used as a projectile in impact tests for the validation of the material models. Both ice samples were made of distilled water. The mould used for the sample preparation is presented in Fig. 1a, which contains two aluminium inserts, rigid cover, and a foundation. The aluminium inserts were used to produce flat ended ice samples, which were fixed on the rigid foundation. The two aluminium inserts were closed with tape and distilled water was injected through a hole in the tape. This method prevents the inclusion of air during the injection of water, but also serves to remove extra liquid water during the freezing process. The mould was assembled by screws to avoid movements of the components. The temperature of the freezer was set to -15°C and the samples were kept in the freezer for 2.5 h. Prior to testing, cylinder ice samples were checked for their transparency, and samples with low transparency were removed as higher transparency indicates fewer micro cracks inside the ice samples. Some qualified samples with high transparency are shown in Fig. 1b, the size of which is $\Phi 15 \times 10$ mm. Regarding the sphere ice samples for impact tests, a similar mould was used as the one for the cylinder samples but with a sphere shape. The sphere ice samples which were frozen for at least 3 h at -15°C are shown in Fig. 1c, the diameter of which is 30 mm. After manufactured, the ice was observed for microstructure, and the grain size of the ice was found to be 0.4-1.6 mm.

2.2. Experimental setup

The experimental setup of the current work, including tensile, compressive and impact tests, is introduced in this section.

2.2.1. Tensile tests

Low strain rates ranging from 10^{-4} to 10^{-1} /s were firstly considered in the present work. A universal electronic testing machine was used, as shown in Fig. 2, to perform Brazilian tests to obtain the tensile properties of the ice samples. In order to keep the samples in low temperature environment, a cooling chamber with liquid nitrogen applied was used and the inner temperature was monitored by a thermometer. A digital camera was placed in front of the samples to record the failure process.

2.2.2. Compressive tests

Considering the dynamic compressive tests, a split Hopkinson bar made of aluminium was used to achieve the strain rate up to 300 /s, while the universal electronic testing machine was employed for tests under quasi-static condition ($\sim 10^{-1}$ /s). More details of the Hopkinson bar can be found in [10,13,34]. For each test, the balanced loading condition and the constant strain rate state have been checked. Otherwise, the experimental results must be discarded for the further use. As in tests under quasi-static condition, a chamber with liquid nitrogen was utilised to maintain the temperature at around -15°C ($\pm$ 2°C) during the compressive tests (Fig. 3).

2.2.3. Impact tests

Regarding the impact tests, the experimental setup is presented in Fig. 4a. An aluminium target made of Al6061 was fixed by steel window frames on both sides, as shown in Fig. 4b. The reason for using aluminium panels as targets is because aluminium is a reliable material model for high-velocity impact cases [35] allowing to focus on studying the capabilities of the material models of ice. Two infrared screens were placed in front of the target to measure the impact velocity of ice projectiles. The ice projectiles were fired with a gas gun placed in front of the target. During the firing process, a sabot (Fig. 4c) was used to protect the ice projectiles from the friction with the gas gun and to control the impact position. Before the projectile touches the target, the sabot was removed with a specific device. A camera on the side of the target was used to make sure the sabot had no effect for the ice impact test. The impact velocity was set at around 100 m/s. Two high-speed cameras with the stereo DIC system applied were placed behind the target to monitor the out of plane deformation; frequency was set to 20 kHz for the deformation history of the target. Data elaboration was conducted by ARAMIS software. Each impact test was repeated at least three times, the representative one has been reported in the current work for the

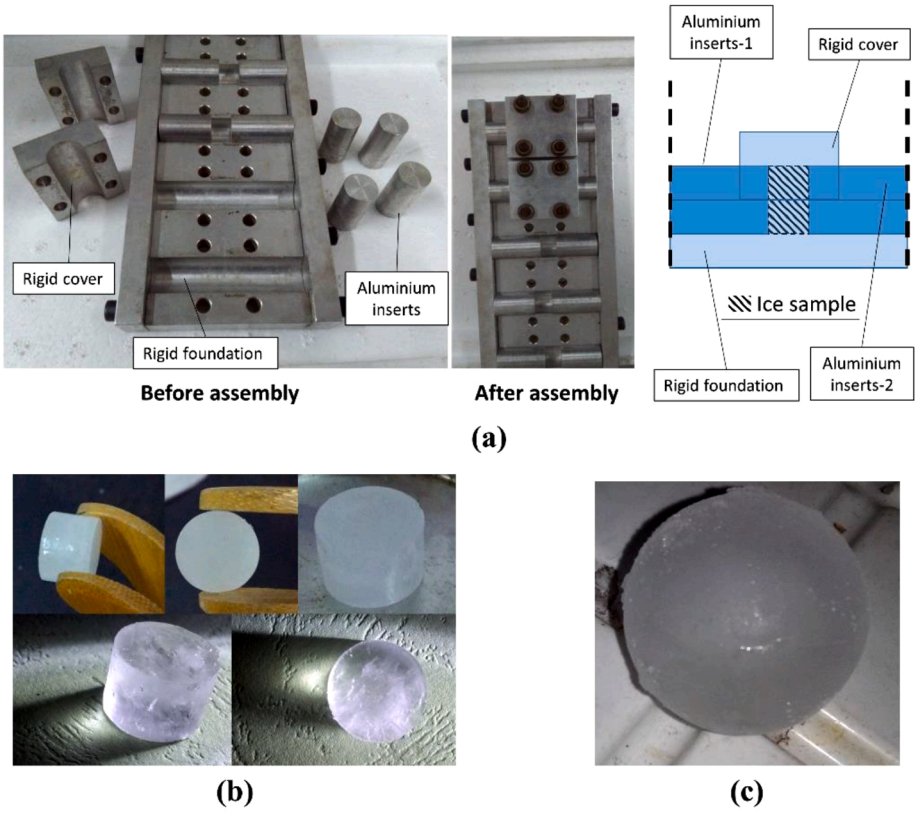

Fig. 1. Components and assembly for cylinder ice samples used in material characterization (a); cylinder ice samples (b); sphere ice samples (c).

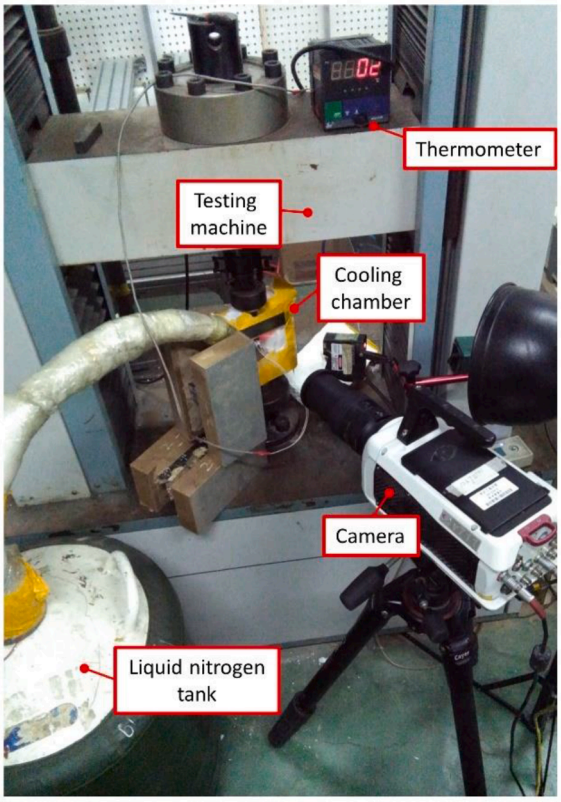

Fig. 2. Experimental setup for quasi-static material tests.

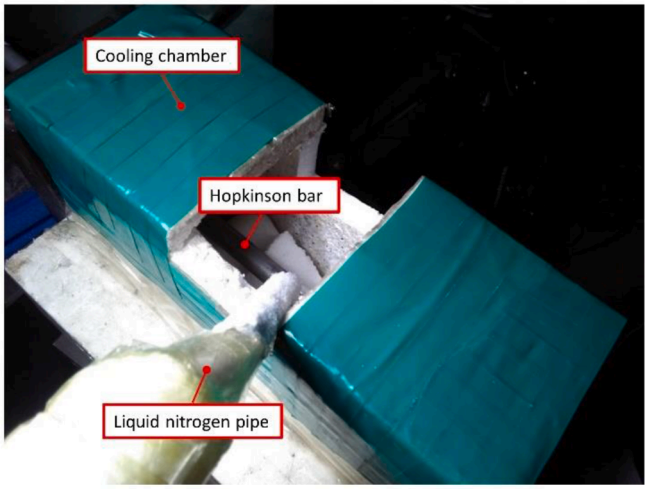

Fig. 3. Cooling chamber designed for split Hopkinson bar test.

validation with the numerical model.

3. Material models

3.1. Test data

In this section, the results from both tensile and compressive tests were regarded as the input for material modelling.

3.1.1. Tensile tests

In the current study, Brazilian tests were conducted with various loading rates to determine the tensile strength of ice. An example of a

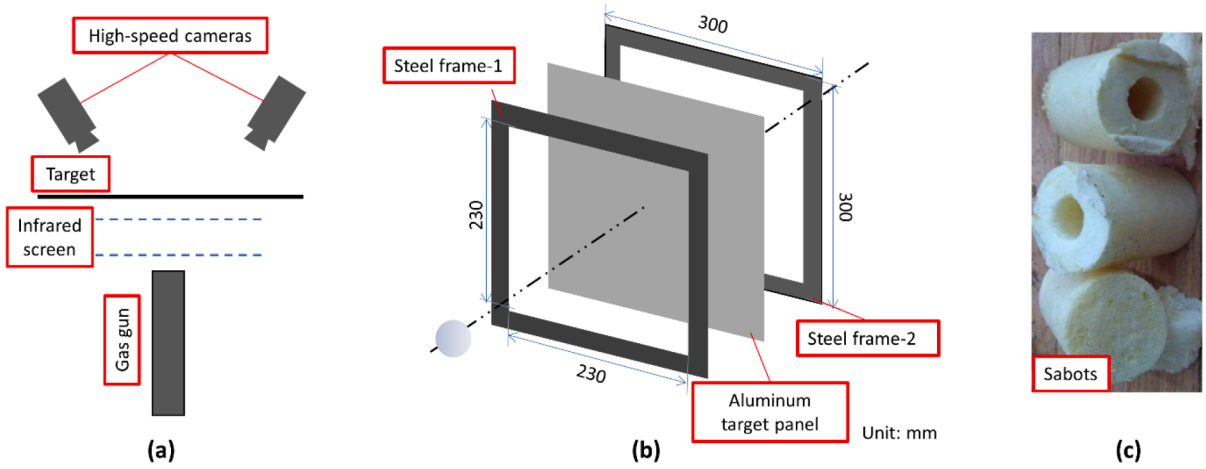

Fig. 4. Experimental setup for ice impact tests (a); scheme about the champs of the targets in the impact tests (b); sabots used in impact tests (c).

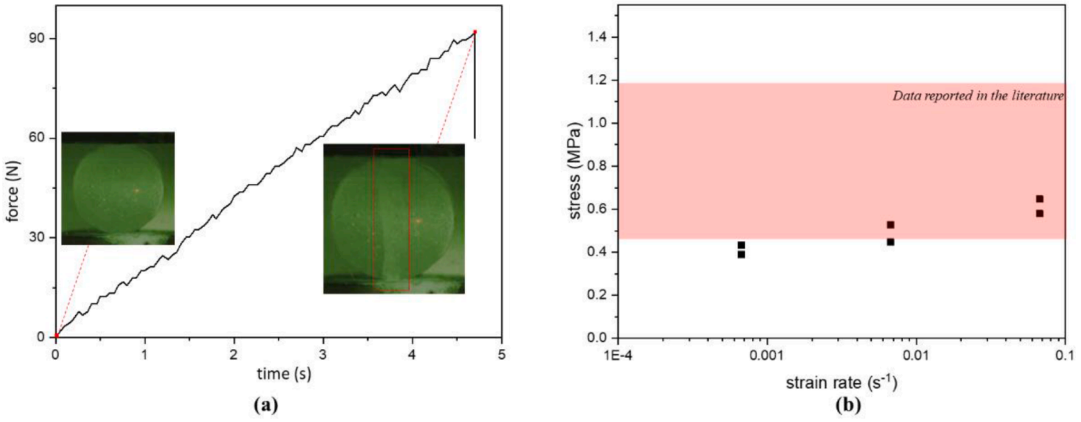

Fig. 5. Typical tensile results with failure process recorded (a); tensile strength under different strain rates (points) and the range of the tensile strength reported in the literature (coloured area) (b).

typical curve from the Brazilian test is shown in Fig. 5a, the sample started cracking at the centre when stress reached the peak, which qualifies the Brazilian tests. The tensile strength test results at different strain rates are presented in Fig. 5b and a 16% increase can be observed from 10^{-4}/s to 10^{-1} /s. Furthermore, the range of the tensile strength reported in the literature is also summarised in Fig. 5b. The strength determined in the current study is then based on the current experimental results from Brazilian tests.

3.1.2. *Compressive tests*

As the strain rate increased, the compressive strength increased up to ~600%, as shown in Fig. 6a. Some typical stress-strain curves under

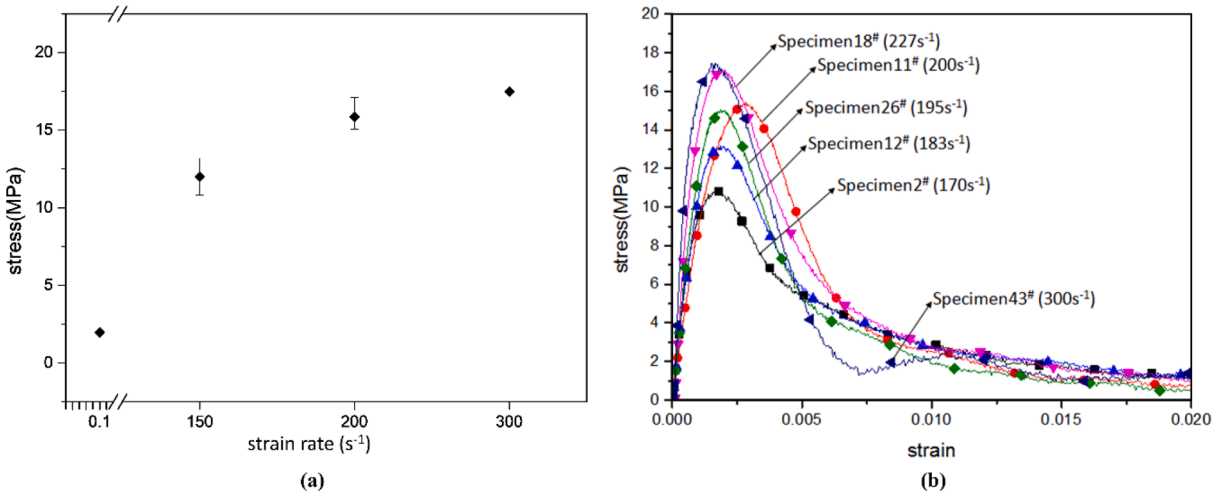

Fig. 6. Typical compressive results of stress-strain curves under different strain rates (a); summary of compressive strengths with respects to strain rates (b).

compression from the split Hopkinson bar tests are shown in Fig. 6b. They can split into three distinct parts: the stress shows a linear increase (part-I); as the yield stress arrives, the stress increases at a gradually slower rate (part-II); after the stress reaches the peak value, the stress starts to drop (part-III), indicating the collapse of the ice sample. Based on these three parts, the material modelling was established.

3.2. Modified Johnson-Cook model

The Johnson-Cook model was first proposed in 1983 [36], and has since been applied in many fields to describe the mechanical behaviours of materials under different loading rates and temperatures. Although this model may not accurately reconstruct the whole deformation history of ice, the mechanical properties under various strain rates and temperatures can be empirically described with a few parameters involved. Coupled with basic mechanical parameters, i.e. elastic modulus and Poisson's ratio (as listed in Table 1), pus the strength model from the Johnson-cook model, the first two parts of the stress-strain curves can be described. In the current work, the compressive strength under different strain rates from tests was utilised as the input for the strength model of the Johnson-Cook model. In order to properly establish a material model of ice, a damage model should be also considered to describe the stress dropping after the peak value (part III). Herein, a modified damage model was applied for failure behaviours of ice after reaching the peak force.

3.2.1. Strength model

The basic equation of Johnson-Cook model can be expressed as Eq. (1), where the effect of the temperature was ignored in the present work.

$$\sigma = (A + B\varepsilon^n)(1 + C ln\dot{\varepsilon}^*) \tag{1}$$

Here, σ, ε and $\dot{\varepsilon}$ are stress, strain, and strain rate, respectively. A, B, C and n are constants, which can be obtained from part-II of the stress strain curves under different strain rates. The least squares method (LSM) was applied for these parameters. Considering this material model later serves for ice as projectiles with high impact velocities, and LSM was initially used to focus on dynamic conditions, the curves from high strain rates is required be more accurate compared to the ones under lower strain rates. Table 1 lists the values of these parameters obtained according to the current test results. The fitted and experimental curves are compared in Fig. 7a, showing that this strength model is capable of predicting part-II of the stress-strain relation under compression.

3.2.2. Damage model

The damage behaviour of ice obtained from the stress-strain curves under different strain rates is presented in Fig. 7b. Generally, the damage model is built based on the degradation of elastic modulus, as expressed in Eq. (2), where $E_0^{'}$ and E are initial and damaged elastic modulus, and D is a damage parameter, which can decide the degrading rate of the material.

$$E = (1 - D)E_0^{'} \tag{2}$$

Considering the trend of the stiffness degradation, an exponential damage model was applied for ice, where D was determined by:

$$D = 1 - \left(\frac{\varepsilon_m^0}{\varepsilon_m^{max}}\right)\left\{1 - \frac{1 - exp\left(-\alpha\left(\frac{\varepsilon_m^{max} - \varepsilon_m^0}{\varepsilon_m^f - \varepsilon_m^0}\right)\right)}{1 - exp(-\alpha)}\right\} \tag{3}$$

ε_m^{max}, ε_m^0 and ε_m^f are the maximum, initial and failure strains for the damage region (part-III) of stress-strain curve; α is the parameter controlling the shape of the damage curve. By changing α, it can be found that the damage curves in Fig. 7b can be replicated when $\alpha = 5.732$. The comparison between the fitted damage and the experimental data with respects to the stress-strain curves is reported in Fig. 7c.

In summary, based on the stress-strain curves from compressive tests, parameters of the modified Johnson-Cook model can be fitted as listed in Table 1.

3.3. Johnson-Holmquist II model

The Johnson-Holmquist II model, containing EOS, the strength model and damage model, which have been used to simulate the mechanical behaviour of brittle materials with high velocity [28], were also considered in the current work. With Johnson-Holmquist II model, the failure of the brittle materials under high strain rates can be replicated precisely due to the application of equations of state, which used the volume strain to describe the deformation of the materials. Meanwhile, strength and damage models can determine the initial failure strength and failure process under different loading conditions, respectively.

3.3.1. Equation of state

EOS is a polynomial which is always used to establish the relationship between pressure and volume strain. At low velocity, a one-order polynomial can provide acceptable accuracy due to the low hydrostatic pressure. However, in the present study, a three-order polynomial was utilised considering the scenario of ice projectiles under high impact velocity, as expressed by Eq. (4). Herein, p is the pressure of ice, and ϵ is the volume strain, while K_1 is the volume modulus, K_2 and K_3 are constants.

$$p = K_1\varepsilon + K_2\varepsilon^2 + K_3\varepsilon^3 \tag{4}$$

K_1 can be obtained through Eq. (5) by elastic modulus E and Poisson's ratio ν of ice.

$$K_1 = E/3(1 - 2\nu) \tag{5}$$

The fitting of K_2 and K_3 is not straightforward as no experiments on pressure and volume strain were conducted. However, the fitting can be obtained mathematically according to the expansion of Hugoniot equation (Eq. (6)) at ϵ, as expressed by Eq. (7).

$$p = \frac{\rho_0 c_0^2 \eta}{(1 - s\eta)^2} \tag{6}$$

$$\begin{cases} K_1 = \rho_0 c_0^2 \\ K_2 = \rho_0 c_0^2 (2s - 1) \end{cases} \tag{7}$$

Thus, the relationship between K_1 and K_2 can be obtained:

$$K_2 = K_1(2s - 1) \tag{8}$$

According to the experimental work from Sterwart and Ahrens [29, 30], $s = 0.92$, is used to calculate K_2 in the current work, whereas K_3, was set as zero because the volume strain should be negligible for ice, as brittle materials always have low failure strength.

After the failure initiation of ice, the radial strain significantly increases causing non-uniform bulking, and leading to the increase of pressure providing internal energy. Thus, the energy transfer parameter, β, and the increment of the pressure, Δp, were used to calibrate the material behaviour in Johnson-Holmquist II model, as listed in Eq. (9). It

Table 1
Parameters for Johnson-Cook model considering damage of ice.

Basic mechanical parameters		Johnson-Cook model		Damage model	
E [GPa]	12	A [MPa]	3.412	α	5.732
ν	0.22	B [MPa]	77.85		
		N	0.355		
		C	0.8593		

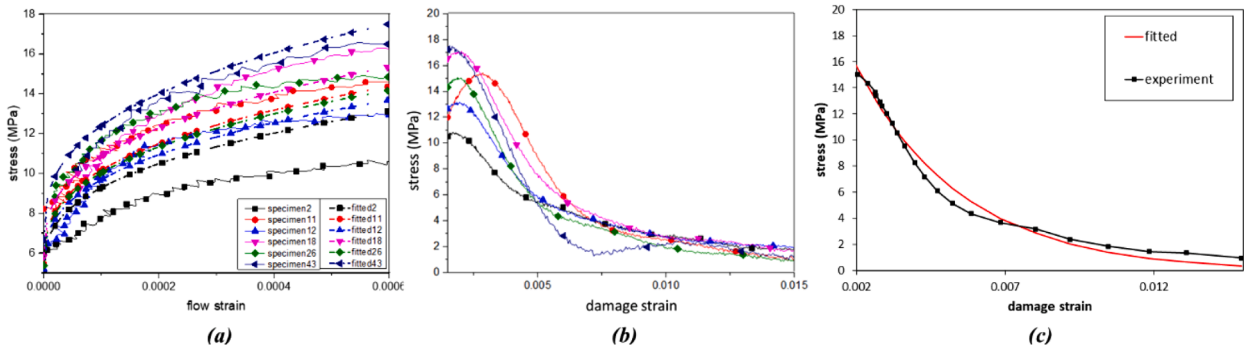

Fig. 7. Comparison between the experimental and fitted curves of part-II (a); part-III of stress-strain curves from tests used for the damage model determination (b); Comparison between the experimental and fitted curves of part-III (strain rate equal to 195 /s).

describes the relationship between the increment of energy and pressure at a specific time interval, Δt. For modelling ice as a projectile, its deformation occurs in a short period. Thus, an unchangeable internal energy can be assumed during the whole process. Then, we could set $= 1$.

$$(\Delta p_{t+\Delta t} - \Delta p_t)\varepsilon_{t+\Delta t} + \left(\Delta p_{t+\Delta t}^2 - \Delta p_t^2\right)/(2K_1) = \beta \Delta U \tag{9}$$

3.3.2. Strength model

In the strength model of Johnson-Holmquist II model, the strain rate effect ($\dot{\varepsilon}$) and damage parameter (D) are considered with the strength normalized by hydrostatic pressure. The normalized parameters are marked with '*' in the strength model (Eqs. (10)-(12)).

$$\sigma^* = \sigma_i^* - D\left(\sigma_i^* - \sigma_f^*\right) \tag{10}$$

When there is no damage ($D = 0$), Eq. (10) can be expressed as:

$$\sigma_i^* = A\left(p^* + \sigma_{t,m}^*\right)^N [1 + Cln(\dot{\varepsilon} / \dot{\varepsilon}_0)] \tag{11}$$

When the material collapses ($D = 1$), σ_f^* can be stated as:

$$\sigma_f^* = B(p^*)^M [1 + Cln(\dot{\varepsilon} / \dot{\varepsilon}_0)] \tag{12}$$

In the strength model, some parameters depend on the material itself, i.e. *A, B, C, N, M*, and the maximum hydrostatic pressure, $\sigma_{t,m}^*$, are introduced. Furthermore, the normalised pressure (p^*) and maximum hydrostatic pressure ($\sigma_{t,m}^*$) in Eqs. (11), (12) are: $p^* = p/p_{HEL}$ and $\sigma_{t,m}^* = \sigma_{t,m}^*/p_{HEL}$.Here, p_{HEL} is the hydrostatic pressure of Hugoniot elastic strength, and it can be expressed by Hugoniot elastic strength. According to the planetary impact tests conducted by Sterwart and Ahrens [29,30], Hugoniot elastic strength, σ_{HEL}, can be fixed to 5.2 GPa for ice. Based on the theory of solid mechanics, the stress can be decomposed in a form of hydrostatic stress and deviator stress tensors as:

$$\sigma_{HEL} = p_{HEL} + \frac{2}{3}s_{HEL} \tag{13}$$

Furthermore, according to Hooke law, the relationship between the deviator stress tensor (s) and volume strain (ε) can be found as:

$$s = 2G\frac{\varepsilon}{1+\varepsilon} \tag{14}$$

Substituting Eqs. (4), (14) into Eq. (13) can obtain:

$$\sigma_{HEL} = K_1\varepsilon_{HEL} + K_2\varepsilon_{HEL}^2 + K_3\varepsilon_{HEL}^3 + \frac{4}{3}G\frac{\varepsilon_{HEL}}{1+\varepsilon_{HEL}} \tag{15}$$

Considering the shear modulus: $G = \frac{E}{2(1+\nu)}$ in Eq. (15), we can get the volume strain at Hugoniot elastic strength $\varepsilon_{HEL} = 0.423$. Therefore, $p_{HEL} = 3.44GPa$ according to Eq. (13).

Moreover, the strength model of Johnson-Holmquist II is based on the increment of strain rate and hydrostatic pressure, but the strength can be also determined by the stress state in reality, which may cause error. Thus, a maximum failure strength, $\sigma_{f,m}$, should also be set to guarantee the capability of the strength model.

Table 2
Normalised parameters used to fit strength model from our experimental activities.

Specimen ID	Strain rate (s^{-1})	σ (MPa)	p (MPa)	σ^*	p^*
2	170	10.79763	3.599211	0.002076468	0.001047
12	183	13.17108	4.390359	0.002532899	0.001277
26	195	15.05995	5.019982	0.002896143	0.00146
18	227	17.11044	5.703479	0.003290469	0.001659

According to our compressive test results, the related parameters are calculated as listed in Table 2 as there is almost no deviated volume deformation in the elastic region for ice samples under uniaxial compression. Thus, we could get: A=1.40, C=0.2287 and N=0.8918, when we used 100 s^{-1} as the reference strain rate.

However, B and M for the strength model after collapse of ice were hard to determine based on existing experimental data, so we utilised B=0.09 and M=1.20 for ice, which have been previously applied on typical brittle materials [37]. Furthermore, the static tensile strength is also employed to determine the tensile failure in the material model, which is set as 1.0 MPa. Herein, a higher tensile strength than the current test results was used in the model considering it is a limit value in the material model for tensile failure.

3.3.3. Damage model

Additionally, to EOS and the strength model, a damage model also has to determine the post-peak behaviour of stress-strain curves. It can be defined by failure strain of the material, ε_f, as presented in Eq. (16), where two damage parameters are introduced: D_1 and D_2. The failure strain here is used to determine the erosion of the elements in the model.

$$\varepsilon_f = D_1\left(p^* + \sigma_{t,max}^*\right)^{D_2} \tag{16}$$

However, those two damage parameters are difficult to obtain experimentally due to the low strain level of the brittle materials. Instead, an inverse modelling approach can be used to numerically obtain the damage parameters. Similar inverse methods have been used for determining material models of brittle materials by Zhang et al. [38]. As for the establishment of the finite element models for the inversion algorithm, experimental cases which are sensitive to the damage behaviours of ice samples should be selected. Therefore, experimental data from the Brazilian tests was used, as the peak force can be reached once the damage initiates.

In detail, to numerically determine the damage parameters, first a finite element model was built to replicate the experimental setup in Brazilian tests, as visible in Fig. 8a. Two platens were created with

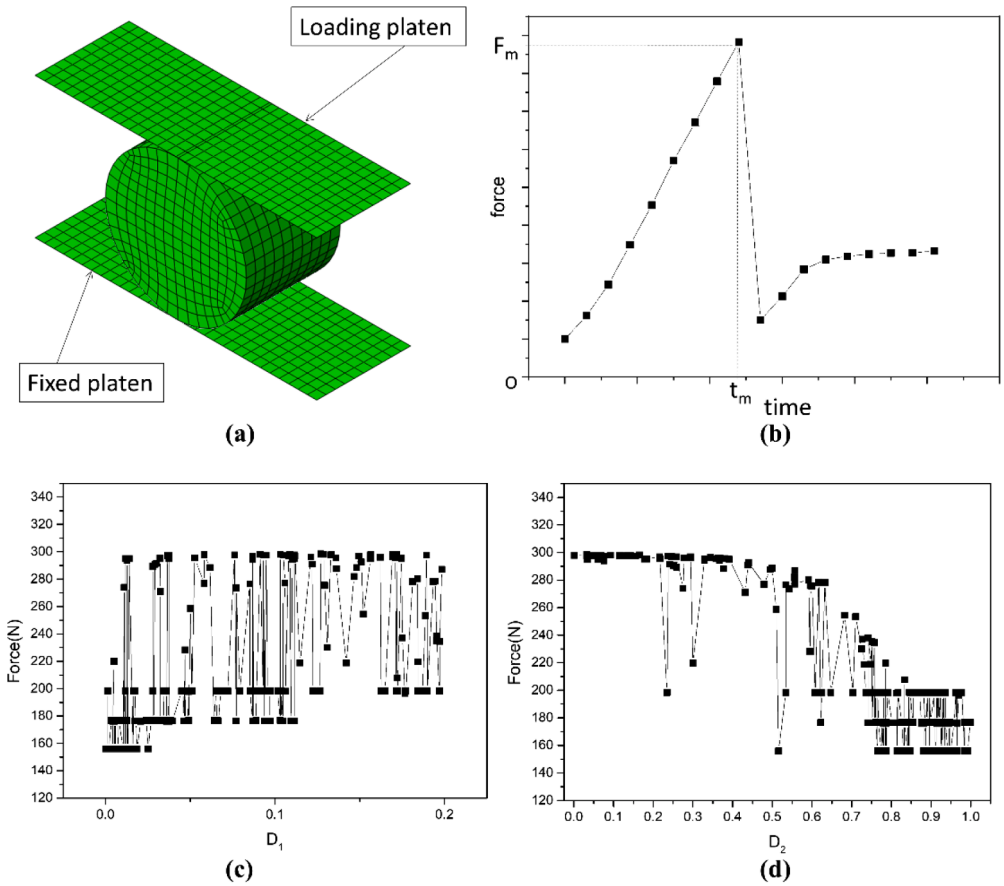

Fig. 8. Inversion finite element method to determine damage parameters: (a) finite element model; (b) typical force-time curve in Brazilian tests; (c) relationship between D_1 and force from inversion calculation; (d) relationship between D_2 and force from inversion calculation.

reduced shell elements (S4R) in ABAQUS. These platens were modelled as rigid bodies during the loading process. The top platen was constrained except along the loading direction at an identical loading rate used in the experiments, while the bottom platen was fixed. Regarding the sample, Johnson-Holmquist II model was assigned in ABAQUS with damage parameters undetermined. The hard contact without friction was assigned between the sample and platens, and the reaction force was extracted for the validation.

Coupled with the software ISIGHT and the automatic modelling strategy, Multi-Island Genetic Algorithms, a global optimization algorithm, was employed to search for suitable damage parameters. The history of the force from Brazilian tests is presented in Fig. 8b. Two important values, i.e. maximum force, F_m, and failure time, t_m, were considered in the algorithm to evaluate different damage parameter values, with the priority on the maximum force, F_m. Herein, 784-time calculation was carried out, and the results of peak forces with various damage parameters are shown in Fig. 8c and 8d. Based on our Brazilian tests, F_m=144.45 N, is the value that can be reached when D_1 closes to zero. Considering D_2, a clear relationship between F_m and D_2 can be found, and a stable F_m can be obtained when D_2 is near one. Besides, t_m was also considered for a good match between experimental data and numerical calculation. Finally, the damage parameters can be determined as: D_1=0.0118 and D_2=0.966.

In summary, the parameters for Johnson-Holmquist II model of ice are in Table 3, based on experimental activities and numerical analysis.

Table 3
Parameters for Johnson-Holmquist II model of ice.

Basic parameters		Equation of state		Strength model		Damage model	
G [MPa]	4444.4	K_1 [MPa]	7058.8	A	1.4	D_1	0.0118
σ_{HEL} [MPa]	5200	K_2 [MPa]	2529.4	C	0.2287	D_2	0.966
P_{HEL} [MPa]	3438.1	K_3 [MPa]	0	N	0.8918		
T_{max} [MPa] (Tensile strength)	1	β	1	B	0.09		
				M	1.2		

4. Validation and assessment of the material models

4.1. Validation of the material models in impact cases with an ice projectile

Impact tests with ice as a projectile and aluminium panel as a target were used to validate the current material models of ice. The mechanical response of targets can be used to evaluate the dynamic mechanical performance of ice projectiles.

4.1.1. Numerical models

The ballistic model was created in ABAQUS, according to the experimental setup of ballistic tests as described in Section 2.2.3. To reduce the modelling and calculation time, the steel frame was modelled through an all-fixed boundary condition in the shadow region of the target, as presented in Fig. 9a. On the other hand, a sphere ice model as the projectile was built with a diameter of 30 mm, as shown in Fig. 9b. The target was modelled with reduced solid elements (C3D8R), while the model of ice projectile was created with integrated solid elements (C3D8) for high accuracy. In total, 30896 solid elements and 41919 nodes were modelled in this ballistic model. A general hard contact was employed between the target and ice, while extra attention was also paid to the contact behaviour among the inner elements of ice. The impact velocity was set as 98 m/s according to the experiments.

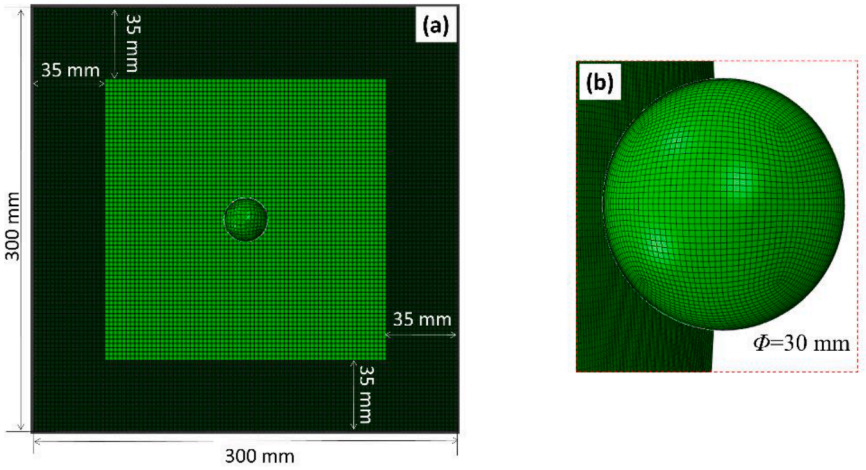

Fig. 9. Finite element model for ballistic tests with ice (a); and details about ice projectile (b).

Table 4
Material model for aluminium (Al6061) [35].

Basic parameters		Johnson-Cook material model	
E [GPa]	70	A [MPa]	60
ν	0.3.	B [MPa]	500
ρ [kg·m^3]	2700	n	0.3
		C	0.02
		Referenced strain rate	1

With regards to the material models, two different models were applied on the ice projectile in the current study: the modified Johnson-Cook model (JC) and Johnson-Holmquist II model (JH), as described in Section 3.2 and Section 3.3. As for the aluminium target, Johnson-Cook model was used, and the parameters for the material model can be obtained from [35] as listed in Table 4.

4.1.2. Numerical and experimental results

Good agreement on the displacement history in the centre of the target, see Fig. 10a, was seen between experiments and simulations using different material models, especially with regards to the increasing trends. Furthermore, similar peak values of the out-of-plane deformation (~ 6.6 mm) and contact time (~ 1.5 ms) were determined. For the two different material models of ice calibrated, the deformation history of target was almost identical based on the DIC results, the deformation at different locations of the target can be extracted. So, the global deformation of the targets at different time points (t=0.2, 0.35, and 0.7 ms) were shown in Fig. 10b. Results from experiments and simulations are in good agreement as far as the displacement history, especially at the initial (0.2 ms) and middle (0.35 ms) moment. However, at 0.7 ms the target centre a larger deformation can be found in simulations than in experiments, indicating a faster damage of the projectile, because the ice projectile used in experiments always contained some defects resulting from the manufacturing process leading to an earlier drop on the displacement as presented in Fig. 10a. Regarding the differences between simulations with two different material models of ice, JC provided a higher deformation at the centre and a lower deformation far from the centre than JH at the initial contact time of 0.2 ms. This indicates that a larger plasticity is provided by JC. However, such differences were reduced as the contact time increases as shown in Fig. 10b. Global displacement fields can also be extracted from DIC, as presented in Fig. 11. Herein, only the numerical results with JH are presented considering the similar numerical results from both material models. A circle displacement field can be found when t = 0.2 ms and t = 0.35 ms, which is similar to the numerical results. However, a rectangular displacement field emerges at t = 0.7 ms caused by the reflected stress wave from the boundary under impact loading, while such behaviour is postponed in the numerical model according to Fig. 11. Overall, both

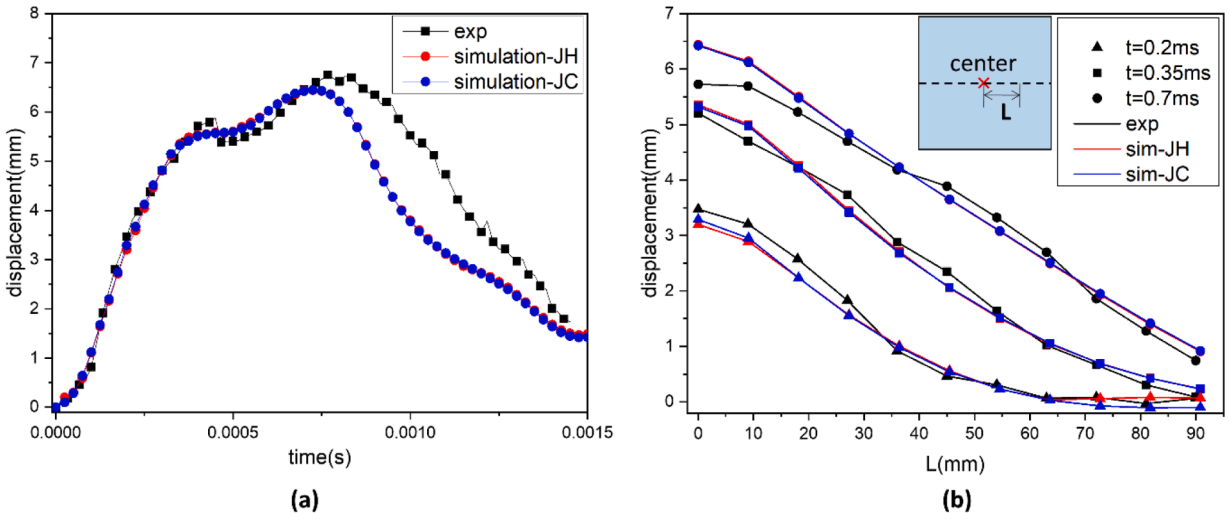

Fig. 10. Comparison of the displacement-time curves obtained from experiments and simulations (a); Comparison of global deformation near the centre of the target between experiments and simulations (b).

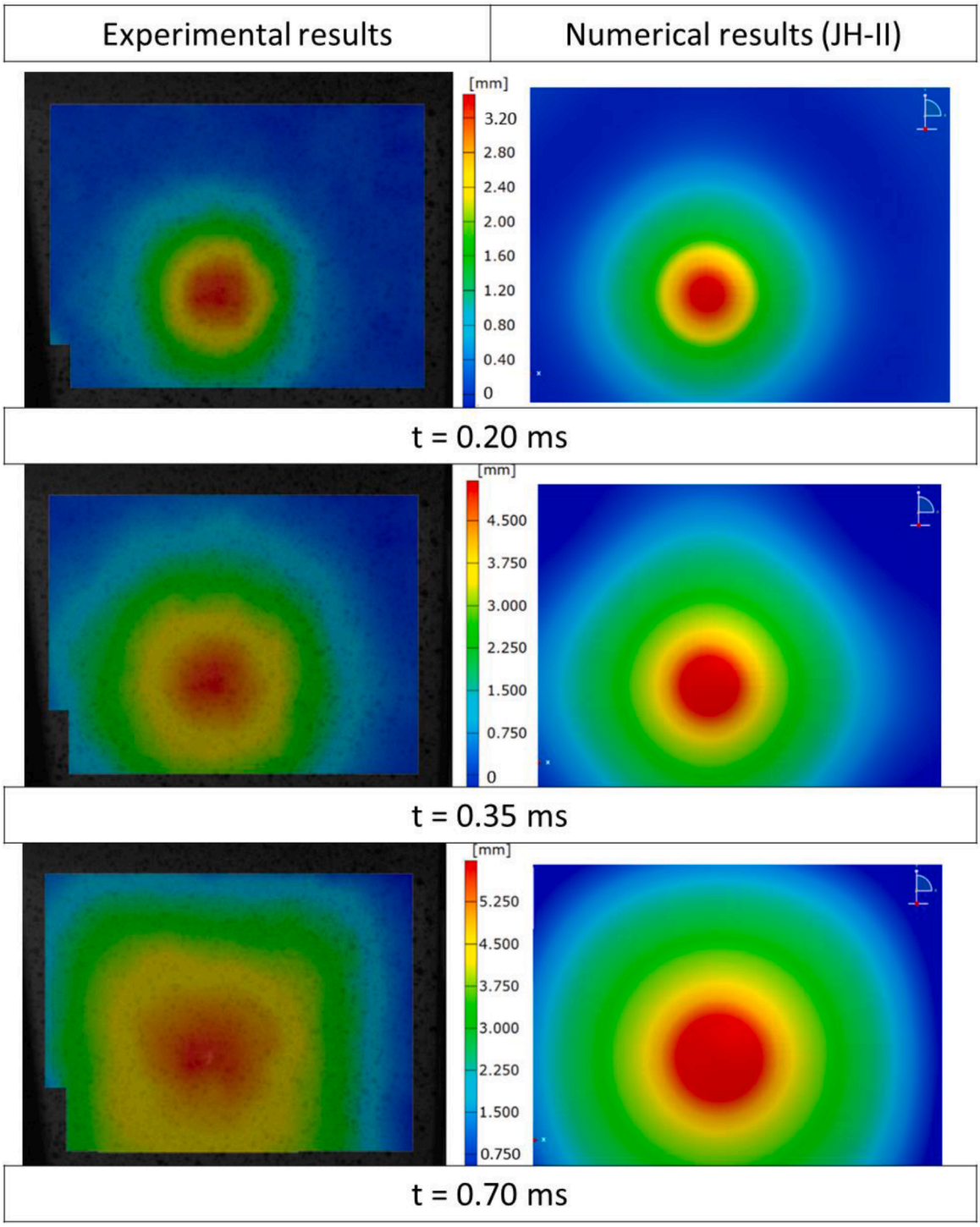

Fig. 11. Comparison of the displacement fields between experiment and simulation at different time steps.

material models of ice are able to replicate the mechanical behaviour of ice as a projectile well.

4.2. Assessment of the different material models

After the validation of both material models, it can be concluded that both material models of ice from the current work are capable to model the ice projectile for a specific velocity and dimension. Therefore, an exploitation of both material models should also be conducted with various dimensions and impact velocities of ice projectiles. Here, the experimental results from Pernas-Sánchez et al. [20] is used, which reported the force between a rigid target and ice projectiles with various dimensions (the diameter equals to 30, 40 and 50 mm) and impact velocities (60 – 220 m/s).

4.2.1. Numerical models

The assessment was conducted with ABAQUS, similar as the validation in section 4.1. Instead of an aluminium target, a rigid target was used by Pernas-Sánchez et al. [20] as presented in Fig. 12. The diameter of the target was 150 mm with the thickness of 0.5 mm, which was meshed with 38270 reduced solid elements (C3D8R). The diameters for the ice projectiles were set as 30, 40 and 50 mm. The ice projectile was

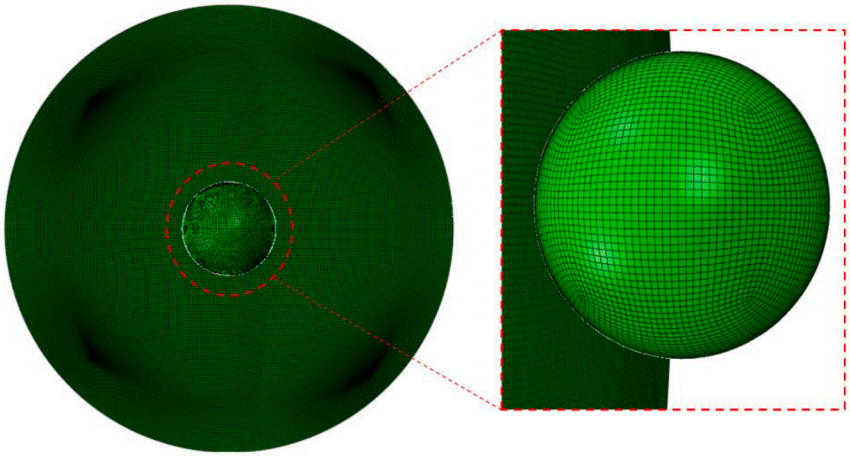

Fig. 12. Finite element model for assessment different material models of ice.

meshed with integrate solid elements (C3D8), which have a similar mesh size as the target in the model, i.e., 0.75 mm, in order to achieve a smooth contact between them. The target was assigned as a rigid body with all freedom fixed. Moreover, general contact was applied for the contact behaviours between the ice projectile and rigid target. An impact velocity was assigned on the ice projectile to simulate the ballistic behaviour.

4.2.2. Numerical and experimental results

The comparison on the force-time curves can be found in Fig. 13. Considering the ice projectile with low input energy (Fig. 13a), i.e., Φ=30 mm, v=98 m/s, good agreement between experimental and numerical results can be found. At this impact energy, JH provides a better prediction than JC of both the peak load and contact time with a limited difference (<15%). The longer contact time from JC was mainly due to the plasticity introduced in JC, which was amplified with a rigid target. Under a high impact energy, i.e., Φ=50 mm, v=211 m/s, the numerical results from both material models are similar, as shown in Fig. 13b. However, they present a higher force than the experimental data as the time increases, indicating the strong dependence of the material model on the impact condition.

Furthermore, the relation between the peak force and the impact energy was investigated for the further assessment of both material models of ice. The maximum contact force from the ice projectile with a 30 mm diameter under different impact energy is presented in Fig. 14a. When the impact energy is less than 150 J, a good match between experiments and simulations can be found for both material models. However, as the energy increases to values greater than 250 J, JH continues to increase whereas both experimental data and JC present a platform (see Fig. 14a). In detail, the experimental contact force has a platform at around 50 kN, while JH simulations result in a platform near 60 kN; however, there is no such behaviour for numerical results with JC. For ice projectiles with a larger diameter (40 mm), higher impact energy and contact force can be achieved as shown in Fig. 14b. The simulation with JH and JC presents a similar correlation with experimental data. Generally, both material models can provide reliable results for ice projectiles with larger dimensions (see Fig. 14a and Fig. 14b). Furthermore, the current numerical results were also compared with other existing experimental data [17,19,20], as shown in Fig. 14c. Considering different impact energies, JH is able to replicate the experimental data for the energy in the range from 0 to 400 J well, while the energy for a good agreement between the numerical model with JC and the experiments is less than 350 J. Overall, JH is more capable than JC with impact energies above 350 J, but considering the large scatter in the experimental measurement, the accuracy of both models of ice is acceptable.

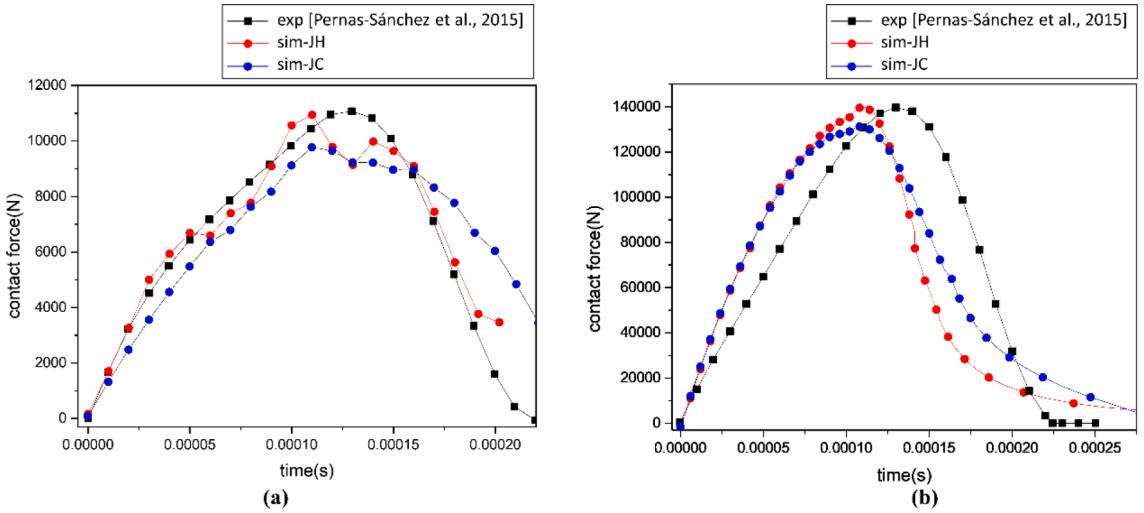

Fig. 13. Comparison of load-time curves between experimental and simulated results under different conditions: (a) Φ=30 mm, v=98 m/s; (b) Φ=50 mm, v=211 m/s

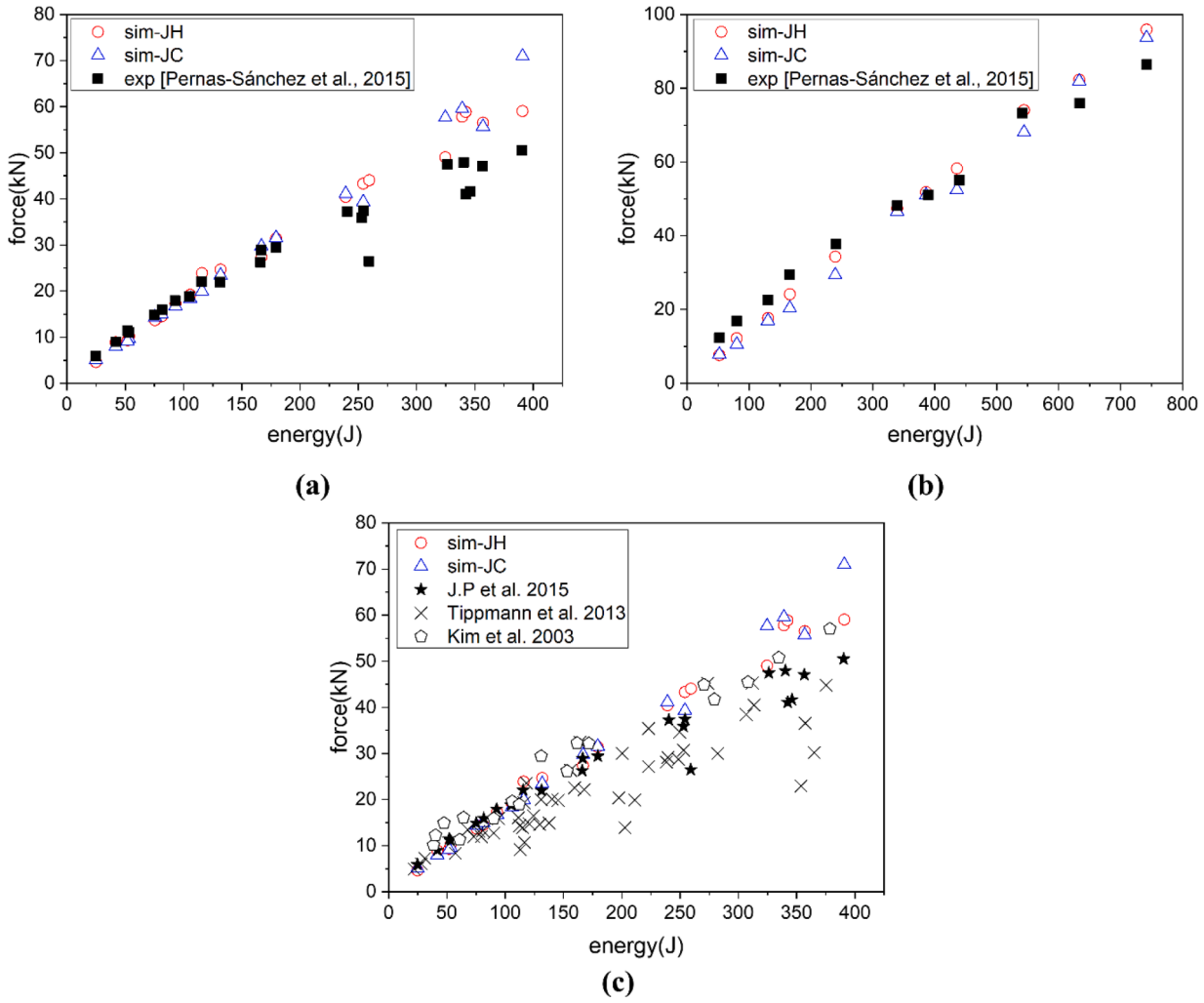

Fig. 14. Comparison on force vs impact energy relationship between experimental and numerical results: (a) diameter of projectile equal to 30 mm; (b) diameter of projectile equal to 40 mm; (c)other experimental data.

4.3. Damage phenomena of ice as a projectile

As the numerical results with JH are more accurate than with JC, the numerical results with JH were used in this section to analyse the damage phenomena of ice as a projectile impacting a rigid target. The experimental recording with a high-speed camera was utilised under intermediate impact energy of our impact case, i.e., Φ=40 mm, v=109 m/s [20]. In order to analyse the damage phenomena of the ice projectile, deleted elements in numerical model were also presented in Fig. 15, which can be regarded as fragments in the experiments. In Fig. 15a, the ice projectile presents less damage compared with experiments at the initial contact period (t = 0.05 ms). A good agreement between simulations and experiments, with respects to the damage volume and the area covered by fragments, can be found later, i.e., near the peak force (t = 0.10 ms) and the force-decreasing region (t = 0.16 ms). Upon reaching the peak force, less than half of the total volume of the ice projectile collapses, similar to the observation from [20]. In the numerical simulation with JH, similar phenomena were noticed as shown in Fig. 15b: the length of the ice projectile along the impact direction is 24.3 mm for the ice projectile with a 40 mm diameter when the load is maximum.

5. Conclusion

In the present work, we carried out experimental activities for the material characterization of ice, including both tensile and compressive tests, considering different strain rates. Based on experimental data, a modified Johnson-Cook model and a Johnson-Holmquist II model were established to describe the mechanical performances of ice in impact cases as a projectile. To validate both material models, impact tests were conducted in the current study. Further, the assessment of both material models was investigated, by comparing the contact force between ice projectiles and impact targets from numerical results and experimental data in the literature. Finally, the damage phenomena of ice projectiles for the impact case conducted in the present work were explored experimentally and numerically. The main conclusions are listed below:

- The strength of ice increases as the strain rate increases, especially the compressive strength.
- Based on the current experimental data, a modified Johnson-Cook model and a Johnson-Holmquist II model, were established aiming to simulate the mechanical behaviours of ice as a projectile.
- Modified Johnson-Cook and Johnson-Holmquist II models can provide reliable results in the ballistic simulation under intermediate impact energy (~350 J).
- Johnson-Holmquist II model can present a good performance in modelling ice impact cases considering the replication of damage phenomena of ice and its loading during impact with high impact energy.

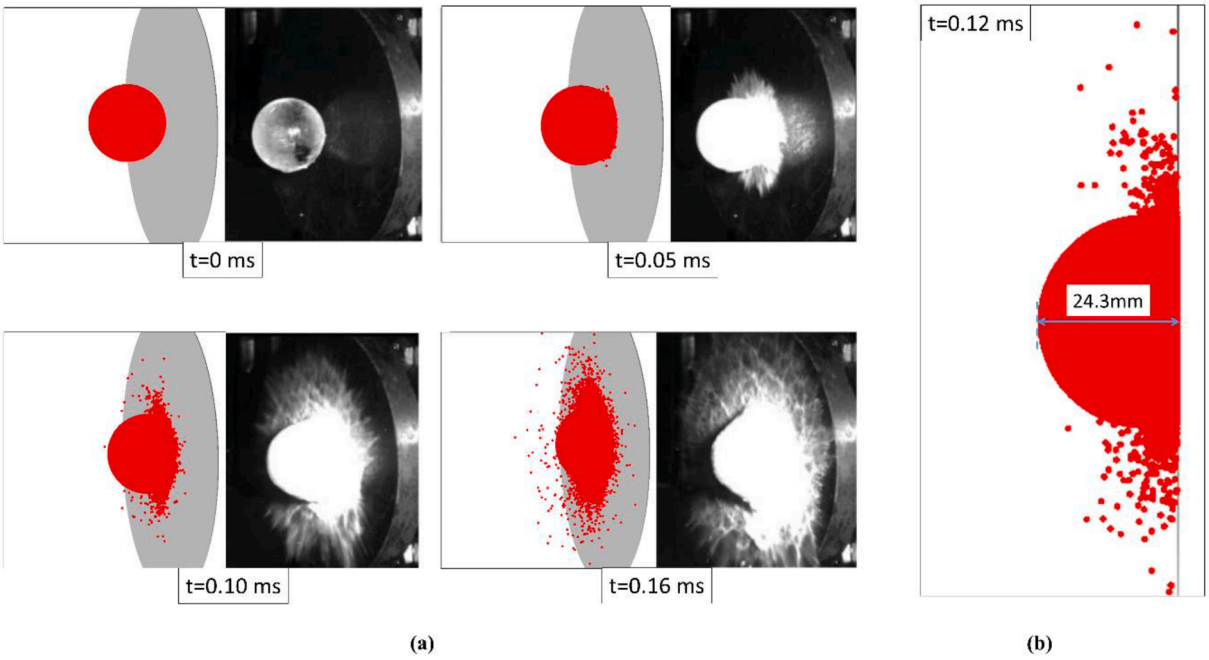

Fig. 15. Damage phenomena of ice impacting to a rigid target: (a) at different time points; (b) at maximum contact force.

CRediT authorship contribution statement

Dayou Ma: Conceptualization, Methodology, Software, Investigation, Validation, Visualization, Writing – original draft. **Xi Li:** Resources, Investigation, Writing – review & editing. **Andrea Manes:** Visualization, Resources, Writing – review & editing. **Yulong Li:** Conceptualization, Writing – review & editing, Supervision, Project administration, Funding acquisition.

Declaration of Competing Interest

The authors declare that they have no known competing financial interests or personal relationships that could have appeared to influence the work reported in this paper.

Data availability

Data will be made available on request.

Acknowledgement

This work was supported by National Natural Science Foundation of China (grant number 11832015).

References

[1] Zhang Y, Wang Q, Han D, Xue Y, Qu J, Yao H. Experimental study of the quasi-static and dynamic fracture toughness of freshwater ice using notched semi-circular bend method. Eng Fract Mech 2021;247:107696. https://doi.org/10.1016/j.engfracmech.2021.107696.
[2] Litwin KL, Zygielbaum BR, Polito PJ, Sklar LS, Collins GC. Influence of temperature, composition, and grain size on the tensile failure of water ice: implications for erosion on Titan. J Geophys Res Planets 2012;117.
[3] Chen X, Ge L, Zhou J, Wu S. Dynamic Brazilian test of concrete using split Hopkinson pressure bar. Mater Struct 2016;50:1. https://doi.org/10.1617/s11527-016-0885-6.
[4] Mohamed AMA, Farzaneh M. An experimental study on the tensile properties of atmospheric ice. Cold Reg Sci Technol 2011;68:91–8. https://doi.org/10.1016/J.COLDREGIONS.2011.06.012.
[5] Zhang Y, Wang Q, Han D, Xue Y, Lu S, Wang P. Dynamic splitting tensile behaviours of distilled-water and river-water ice using a modified SHPB setup. Int J Impact Eng 2020:103686. https://doi.org/10.1016/j.ijimpeng.2020.103686.
[6] Ademović N, Kurtović A. Influence of planes of anisotropy on physical and mechanical properties of freshwater limestone (Mudstone). Constr Build Mater 2021;268:121174. https://doi.org/10.1016/J.CONBUILDMAT.2020.121174.
[7] Hiraoka K, Arakawa M, Setoh M, Nakamura AM. Measurements of target compressive and tensile strength for application to impact cratering on ice-silicate mixtures. J Geophys Res Planets 2008;113.
[8] Saletti D, Georges D, Gouy V, Montagnat M, Forquin P. A study of the mechanical response of polycrystalline ice subjected to dynamic tension loading using the spalling test technique. Int J Impact Eng 2019;132:103315. https://doi.org/10.1016/J.IJIMPENG.2019.103315.
[9] Georges D, Saletti D, Montagnat M, Forquin P, Hagenmuller P. Influence of Porosity on Ice Dynamic Tensile Behavior as Assessed by Spalling Tests 2021;7:575–90. https://doi.org/10.1007/s40870-021-00300-z.
[10] Othman R. The Kolsky-Hopkinson Bar Machine. Cham: Springer International Publishing; 2018. https://doi.org/10.1007/978-3-319-71919-1.
[11] Jones SJ. High Strain-Rate Compression Tests on Ice. J Phys Chem B 1997;101:6099–101. https://doi.org/10.1021/JP963162J.
[12] Kim H, Keune JN. Compressive strength of ice at impact strain rates. J Mater Sci 2007;42:2802–6. https://doi.org/10.1007/S10853-006-1376-X.
[13] Shazly M, Prakash V, Lerch BA. High strain-rate behavior of ice under uniaxial compression. Int J Solids Struct 2009;46:1499–515. https://doi.org/10.1016/J.IJSOLSTR.2008.11.020.
[14] Wu X, Prakash V. Dynamic compressive behavior of ice at cryogenic temperatures. Cold Reg Sci Technol 2015;118:1–13. https://doi.org/10.1016/J.COLDREGIONS.2015.06.004.
[15] Carney KS, Benson DJ, DuBois P, Lee R. A phenomenological high strain rate model with failure for ice. Int J Solids Struct 2006;43:7820–39. https://doi.org/10.1016/j.ijsolstr.2006.04.005.
[16] Karpen N, Cuco A, Kuenstler D, Bonaccurso E, Reitter LM, Roisman IV, et al. AIAA Aviat. 2021 FORUM. Reston, Virginia: American Institute of Aeronautics and Astronautics; 2021. https://doi.org/10.2514/6.2021-2671.
[17] Kim H, Welch DA, Kedward KT. Experimental investigation of high velocity ice impacts on woven carbon/epoxy composite panels. Compos Part A Appl Sci Manuf 2003;34:25–41. https://doi.org/10.1016/S1359-835X(02)00258-0.
[18] Hong YK, Moon KH. Experimental research on ice particle impact on aluminum alloys. Wear 2017;382–383:102–6. https://doi.org/10.1016/j.wear.2017.04.024.
[19] Tippmann JD, Kim H, Rhymer JD. Experimentally validated strain rate dependent material model for spherical ice impact simulation. Int J Impact Eng 2013;57:43–54. https://doi.org/10.1016/J.IJIMPENG.2013.01.013.
[20] Pernas-Sánchez J, Artero-Guerrero JA, Varas D, López-Puente J. Analysis of Ice Impact Process at High Velocity. Exp Mech 2015;55:1669–79. https://doi.org/10.1007/s11340-015-0067-4.
[21] Schoenherr TF. Calculating the Impact Force of Supersonic Hail Stones Using SWAT-TEEM. Conf Proc Soc Exp Mech Ser 2015;9:67–79. https://doi.org/10.1007/978-3-319-15233-2_9.
[22] Hild F, Bouterf A, Roux S. Measurement of kinematic fields via DIC for impact engineering applications. Int J Impact Eng 2019. https://doi.org/10.1016/J.IJIMPENG.2019.04.007.
[23] Sain T, Narasimhan R. Constitutive modeling of ice in the high strain rate regime. Int J Solids Struct 2011;48:817–27. https://doi.org/10.1016/J.IJSOLSTR.2010.11.016.

[24] Ince ST, Kumar A, Paik JK. A new constitutive equation on ice materials. Ships Offshore Struct 2017;12:610–23. https://doi.org/10.1080/17445302.2016.1190122.
[25] Zhang F, Zhu Z, Fu T, Jia J. Damage mechanism and dynamic constitutive model of frozen soil under uniaxial impact loading. Mech Mater 2020;140:103217. https://doi.org/10.1016/J.MECHMAT.2019.103217.
[26] Tang Z, Hang C, Suo T, Wang Y, Dai L, Zhang Y, et al. Numerical and experimental investigation on hail impact on composite panels. Int J Impact Eng 2017;105:102–8. https://doi.org/10.1016/j.ijimpeng.2016.05.016.
[27] Cui Q, Yang J. Evaluation of numerical simulation methods and ice material models for intermediate-velocity hail impact simulation. Eng Struct 2021;244:112831. https://doi.org/10.1016/j.engstruct.2021.112831.
[28] Wang Z, Ma D, Suo T, Li Y, Manes A. Investigation into different numerical methods in predicting the response of aluminosilicate glass under quasi-static and impact loading conditions. Int J Mech Sci 2021:106286. https://doi.org/10.1016/j.ijmecsci.2021.106286.
[29] Stewart ST, Ahrens TJ. Shock Hugoniot of H_2O ice. Geophys Res Lett 2003;30:1332. https://doi.org/10.1029/2002GL016789.
[30] Stewart ST, Ahrens TJ. A new H2O ice hugoniot: implications for planetary impact events. AIP Conf Proc 2004;706:1478. https://doi.org/10.1063/1.1780518.
[31] Zhang JP, Zhou D. Numerical modeling for strain rate effect and size effect of ice under uniaxial tension and compression. Commun Nonlinear Sci Numer Simul 2021;96:105614. https://doi.org/10.1016/J.CNSNS.2020.105614.
[32] Coles LA, Roy A, Silberschmidt VV. Ice vs. steel: ballistic impact of woven carbon/epoxy composites. Part II – numerical modelling. Eng Fract Mech 2019. https://doi.org/10.1016/J.ENGFRACMECH.2018.12.030.
[33] Kabore BW, Peters B. Micromechanical model for sintering and damage in viscoelastic porous ice and snow. Part II: validation. Int J Solids Struct 2020;185–186:281–91. https://doi.org/10.1016/j.ijsolstr.2019.08.036.
[34] Zhao Z, Liu P, Dang H, Nie H, Guo Z, Zhang C, et al. Effects of loading rate and loading direction on the compressive failure behavior of a 2D triaxially braided composite. Int J Impact Eng 2021;156:103928. https://doi.org/10.1016/J.IJIMPENG.2021.103928.
[35] Grignon F, Benson D, Vecchio KS, Meyers MA. Explosive welding of aluminum to aluminum: analysis, computations and experiments. Int J Impact Eng 2004;30:1333–51. https://doi.org/10.1016/j.ijimpeng.2003.09.049.
[36] Johnson GR, Cook WH. Fracture characteristics of three metals subjected to various strains, strain rates, temperatures and pressures. Eng Fract Mech 1985;21:31–48.
[37] Yan SC, Zheng T, Wang HH. Experimental study and numerical simulation on standard blasting crater of ice. Eng Blasting 2011.
[38] Zhang YK, Li YL, Zhang HB. A method to identify bird constitutive model and its parameters. Appl Mech Mater 2013;302:686–93. https://doi.org/10.4028/www.scientific.net/AMM.302.686.